Optimal control of an inhomogeneous spin ensemble coupled to a cavity

Q. Ansel,[1,2] S. Probst,[3] P. Bertet,[3] S. J. Glaser,[1] and D. Sugny[2,4,*]

[1]*Department of Chemistry, Technische Universität München, Lichtenbergstrasse 4, D-85747 Garching, Germany*

[2]*Laboratoire Interdisciplinaire Carnot de Bourgogne (ICB), UMR 6303 CNRS–Université de Bourgogne–Franche Comté, 9 Avenue A. Savary, BP 47 870, F-21078 Dijon cedex, France*

[3]*Quantronics Group, SPEC, CEA, CNRS, Université Paris-Saclay, CEA Saclay, 91191 Gif-sur-Yvette, France*

[4]*Institute for Advanced Study, Technische Universität München, Lichtenbergstrasse 2a, D-85748 Garching, Germany*

We apply optimal-control techniques to an inhomogeneous spin ensemble coupled to a cavity. A general procedure is proposed for designing the control strategies. We numerically show the extent to which optimal-control fields robust against system uncertainties help enhance the sensitivity of the detection process. The parameters of the numerical simulations are taken from recent electron spin resonance experiments. The low and high cooperativity regimes are explored.

I. INTRODUCTION

Quantum optimal control theory (QOCT) is aimed at finding a way to bring a quantum system from one state to another with minimum expenditure of time and resources [1–7]. Intense progress has been realized recently in the development of such techniques [1,2]. Several optimization algorithms [8–11] have been proposed to design control fields suited to different experimental setups and constraints or robust against experimental uncertainties and modeling imperfections [12–20]. QOCT was first developed in molecular physics to steer chemical reactions [2,6,21,22] and in nuclear magnetic resonance (NMR) or magnetic resonance imaging for controlling spin dynamics [8,23–30]. OCT is nowadays attracting a lot of effort in the context of quantum-information processing [31–34] and has been recognized as one of the cornerstones for enabling quantum technologies [1].

In NMR, spin dynamics are governed by the Bloch equation and controlled by a radio-frequency magnetic field which is assumed to be a piecewise constant function adjustable in time. This approximation corresponds to a standard framework in QOCT [8]. The situation is not so simple in electron spin resonance (ESR) and specific experimental constraints due to technical limitations of the spectrometer have to be accounted for. For instance, the role of the microwave resonator cannot be neglected and the field applied to the spins is distorted by the response function of the cavity [35,36]. The main experimental limitation is the nonlinearity of the resonator which arises for large amplitudes of the intracavity field, particularly for superconducting microresonators. In other experimental setups, a continuous variation of the amplitude and phase of the control pulses is not possible and only switches between a discrete set of pulse phases is permitted by the available hardware [37,38]. QOCT has been applied with success in

these different settings [36,39], showing the efficiency and the flexibility of this approach.

The detection of individual spins is a challenging issue in magnetic resonance [40]. Different experimental strategies have been proposed to date to reach this single-spin limit [41–45]. Among other propositions, a promising option is to push to its physical limit the inductive detection method in ESR [46–50]. Recent progress has shown that 260 spins per echo can by now be detected with a signal-to-noise ratio of 1 [50]. This gain of several orders of magnitude in sensitivity over the conventional approaches has been made possible by different experimental advances extending from the cryogenic temperature of the sample to the high quality factor of the microresonators and by the use of Josephson parametric amplifier devices. Hahn echo or Carre-Purcell-Meiboom-Gill (CPMG) sequences [51] are usually implemented with standard rectangular pulses to measure the echo signal emitted by the spins in the cavity [51–53]. However, the efficiency of these control protocols is limited by the response function of the resonator and by the inhomogeneities and imperfections of the sample. In the running to the single-spin detection, it is therefore crucial to identify control procedures enhancing the echo signal for a given number of excited spins. This issue is addressed numerically in this paper by using tools of OCT, which offer the possibility to go beyond intuitive protocols. For the sake of concreteness, the theoretical analysis of this work is based on some recent experiments made in ESR [47–50]. A schematic description of the physical concepts at the basis of the control process in given in Fig. 1. The control of the spin ensemble is a two-step procedure in which only the intracavity field can be directly modified by the external control, the field applied to the spins being distorted by the response function of the resonator. In the case in which the cavity acts as a linear bandpass filter, the cavity response can be deconvoluted and the intracavity field can be designed (up to some extent) for any given field the spins are subjected to. The back-action of the spin ensemble to the cavity adds, in the high-cooperativity regime, a degree of complexity to this control scenario.
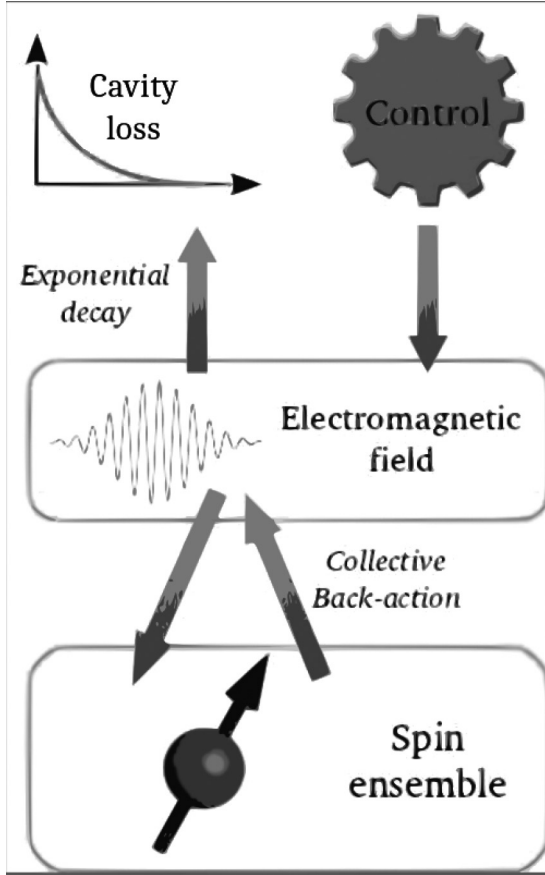
*dominique.sugny@u-bourgogne.fr

FIG. 1. Schematic description of the system (3). The control pulses can only change the electromagnetic field of the cavity and not directly the dynamics of the spins. Note the back-action of the spins onto the cavity mode.

From a theoretical point of view, the quantum dynamics are governed by a damped Jaynes-Cummings model. The optimization procedure presented in this paper is an extension of a standard iterative algorithm, namely GRAPE [8]. We first optimize the field acting on the spin ensemble to realize efficient Hahn and CPMG sequences even if the system parameters are known with a finite precision. The deconvolution of the resonator response leads then to the intracavity field. Specific constraints are accounted for in the optimization process to design realistic fields. We show the efficiency of the corresponding optimal fields for enhancing the signal-to-noise ratio (SNR) of the detection process and its sensitivity, that is, the minimum number of spins per echo that can be detected with a signal-to-noise ratio of 1. Note that closely related works have recently investigated the optimal control of such systems for quantum-information applications (see, e.g., [54–60] to cite a few).

The remainder of this paper is organized as follows. The model system is introduced in Sec. II with special attention paid to the different approximations. Optimal-control techniques and robust control fields are described in Sec. III. Section IV presents numerical results based on recent ESR experiments. We conclude in Sec. V with an outlook and different perspectives. Supplementary data are reported in the Appendix.

II. THEORETICAL DESCRIPTION

A. The model system

We consider an inhomogeneous ensemble of spin-1/2 particles with different resonance frequencies coupled to a single-mode cavity. The parameter values are chosen to be in accordance with recent experiments in ESR [47–50]. The dynamics of the system can be described by the damped Jaynes-Cummings model. In a frame rotating at ω, the frequency of the microwave drive, the density matrix ρ satisfies the following differential equation (in units of $\hbar$):

$$\dot{\rho} = -i[H, \rho] + \mathcal{L}(\rho), \tag{1}$$

where

$$H = \omega_0 a^\dagger a + \sum_{j=1}^{N} \left[\frac{\omega_j}{2} \sigma_z^{(j)} + g_j (a^\dagger \sigma_-^{(j)} + a \sigma_+^{(j)}) \right]$$
$$+ i(\beta a^\dagger - \beta^* a)$$

and

$$\mathcal{L}(\rho) = \kappa \left(a\rho a^\dagger - \tfrac{1}{2}\rho a^\dagger a - \tfrac{1}{2}a^\dagger a\rho \right).$$

The parameters ω_0 and ω_j are respectively the detunings of the cavity and of the spins with respect to the drive frequency of the field. We denote by N the number of spins in the ensemble. A specific example will be investigated in Sec. IV. The coupling strength between each spin and the cavity is given by the constant g_j. The amplitude of the microwave drive applied to the cavity mode is represented by the time-dependent functions $\beta(t)$ and $\beta^*(t)$. The cavity losses are described by the Lindbladian $\mathcal{L}$ with a rate κ. We recall the standard commutation relations between the different operators: $[a, a^\dagger] = 1$, $[\sigma_x, \sigma_y] = 2i\sigma_z$, $[\sigma_+, \sigma_-] = \sigma_z$, $[\sigma_z, \sigma_\pm] = \pm 2\sigma_\pm$, $\sigma_x = \sigma_+ + \sigma_-$, and $\sigma_y = -i(\sigma_+ - \sigma_-)$. Using Eq. (1), it is straightforward to show that the time evolution of the expectation values of the different operators, denoted $\langle \cdot \rangle$, is governed by

$$\frac{d}{dt}\langle \hat{X} \rangle = -\omega_0 \langle \hat{Y} \rangle - \frac{\kappa}{2}\langle \hat{X} \rangle + \omega_X - \sum_j 2g_j \langle \hat{S}_y^{(j)} \rangle,$$

$$\frac{d}{dt}\langle \hat{Y} \rangle = \omega_0 \langle \hat{X} \rangle - \frac{\kappa}{2}\langle \hat{Y} \rangle + \omega_Y + \sum_j 2g_j \langle \hat{S}_x^{(j)} \rangle,$$

$$\frac{d}{dt}\langle \hat{S}_x^{(j)} \rangle = -\omega_j \langle \hat{S}_y^{(j)} \rangle + g_j \langle \hat{Y} \hat{S}_z^{(j)} \rangle,$$

$$\frac{d}{dt}\langle \hat{S}_y^{(j)} \rangle = \omega_j \langle \hat{S}_x^{(j)} \rangle - g_j \langle \hat{X} \hat{S}_z^{(j)} \rangle, \tag{2}$$

$$\frac{d}{dt}\langle \hat{S}_z^{(j)} \rangle = g_j \langle \hat{X} \hat{S}_y^{(j)} \rangle - g_j \langle \hat{Y} \hat{S}_x^{(j)} \rangle,$$

where we have introduced the operators $\hat{S}_{x,y,z,\pm}^{(j)} = \sigma_{x,y,z,\pm}^{(j)}/2$, $\hat{X} = a + a^\dagger$, and $\hat{Y} = -i(a^\dagger - a)$ in order to get more symmetrical expressions. The control fields are given by the two real functions $\omega_X = \beta + \beta^*$ and $\omega_Y = i(\beta - \beta^*)$.

From now on, we consider different degrees of approximation which lead to numerical optimizations computationally less expensive. These approximations are widely used in quantum optics [61]. A first approximation consists of neglecting quantum correlations between the spins and the

cavity mode. This approximation can be introduced in the framework of cumulant expansion [62,63]. In this work, we consider an expansion of order two in which $\langle \hat{A}\hat{B} \rangle \simeq \langle \hat{A} \rangle \langle \hat{B} \rangle$. This approximation is justified in the bad-cavity limit and it greatly simplifies the differential system which becomes of dimension $3N + 2$. In the frame rotating at frequency ω_0, we have

$$\dot{X} = -\frac{\kappa}{2}X + \omega_X - \sum_j 2g_j S_y^{(j)},$$

$$\dot{Y} = -\frac{\kappa}{2}Y + \omega_Y + \sum_j 2g_j S_x^{(j)},$$

$$\dot{S}_x^{(j)} = -\Delta_j S_y^{(j)} + g_j Y S_z^{(j)}, \qquad (3)$$

$$\dot{S}_y^{(j)} = \Delta_j S_x^{(j)} - g_j X S_z^{(j)},$$

$$\dot{S}_z^{(j)} = g_j X S_y^{(j)} - g_j Y S_x^{(j)},$$

where we use (for the sake of simplicity) the same notations $A = \langle \hat{A} \rangle$ for the observable A in the initial and the rotating frames. For each spin, we introduce the offset $\Delta_j = \omega_j - \omega_0$. In Eq. (3), X, Y, ω_X, ω_Y, and $\vec{S}^{(j)}$ are expressed in dimensionless units. A straightforward physical interpretation of the dynamics can be given from Eq. (3). Equation (3) describes an ensemble of spins coupled to a driven classical oscillator, whose dynamics depend on the state of the spins. In particular, we obtain that the spins move along the Bloch sphere, $\vec{S}^{(j)}(t)^2 = \text{cst}$. This description is illustrated in Fig. 1. This situation is similar to the one encountered in magnetic resonance when the detection coil induces a back-action on the spins. This well-known effect, called the radiation damping effect, is modeled by nonlinear terms in the Bloch equation governing the spin dynamics [64–67]. This modeling can be recovered from Eq. (3) in the bad-cavity limit discussed in Sec. II B where $g \ll \kappa$ [68–73].

The spin ensemble is also subjected to standard T_1 and T_2 relaxation processes. The interaction of the spins with the cavity leads to another T_1-relaxation process, called the Purcell effect [48,61,74], which can be interpreted as a cavity-enhanced spontaneous emission. The corresponding relaxation time T_1^p can be expressed as

$$\frac{1}{T_1^p} = \frac{\kappa g_i^2}{\Delta_j^2 + \kappa^2/4}. \qquad (4)$$

Note that spins detuned from the cavity have a longer relaxation time and that $T_1^p \ll T_1$ in the experimental situation we consider in this work.

Finally, we point out that some collective effects of the spin ensemble, such as super-radiant relaxation, governed by the Tavis-Cummings Hamiltonian [75] occur if the offset inhomogeneities are not too strong [76–78]. The transition between the individual and collective spin regimes is described by the cooperativity parameter C. In the case of a spin ensemble with a Lorentzian density of frequencies of full width at half height Ω, the parameter C can be expressed as $C = \frac{2Ng^2}{\kappa\Omega}$ [77].

B. The bad-cavity limit

We recall in this section the standard approximation of the bad-cavity limit. We first integrate the two first equations of

(3) and we obtain

$$X(t) = \int_{-\infty}^t e^{-\frac{\kappa}{2}(t-t')} C_X(t') dt',$$

$$Y(t) = \int_{-\infty}^t e^{-\frac{\kappa}{2}(t-t')} C_Y(t') dt', \qquad (5)$$

with $\quad C_X(t') = \omega_X(t') - 2\sum_j g_j S_y^{(j)}(t') \quad$ and $\quad C_y(t') = \omega_Y(t') + 2\sum_j g_j S_X^{(j)}(t')$. We define the integral F of a function f,

$$\mathsf{F} = \int_{-\infty}^t e^{\frac{\kappa}{2}(t'-t)} f(t') dt',$$

the goal being to compute the limit of F when $\kappa \to +\infty$. For that purpose, we define a sequence of functions μ_k,

$$\mu_k(t) = \frac{\kappa_k}{4} e^{-\kappa_k |t|/2},$$

which converges towards the Dirac distribution if $\kappa_k \to +\infty$ when $k \to +\infty$. From the relations of generalized function theory which involve the product of a Dirac distribution with a Heaviside function [79], we obtain that

$$\mathsf{F} \simeq \frac{2}{\kappa} f(t),$$

when $\kappa \gg 1$ [κ is expressed here in the dimensionless units of Eq. (3)]. This approximation leads to

$$X(t) = \frac{2}{\kappa}\left(\omega_X - 2\sum_j g_j S_y^{(j)} \right),$$

$$Y(t) = \frac{2}{\kappa}\left(\omega_Y + 2\sum_j g_j S_x^{(j)} \right). \qquad (6)$$

Plugging (6) into (3), we arrive at

$$\dot{S}_x^{(j)} = -\Delta_j S_y^{(j)} + \frac{2g}{\kappa}\omega_Y S_z^{(j)} + \frac{4g^2}{\kappa}\bar{S}_x S_z^{(j)},$$

$$\dot{S}_y^{(j)} = \Delta_j S_x^{(j)} - \frac{2g}{\kappa}\omega_X S_z^{(j)} + \frac{4g^2}{\kappa}\bar{S}_y S_z^{(j)}, \qquad (7)$$

$$\dot{S}_z^{(j)} = \frac{2g}{\kappa}\left[\omega_X S_y^{(j)} - \omega_Y S_x(j) \right] - \frac{4g^2}{\kappa}\left(\bar{S}_x S_x^{(j)} + \bar{S}_y S_y^{(j)} \right),$$

where $g_j = g$ is assumed to be the same for all the spins and $\bar{S}_x = \sum_k S_x^{(k)}$, $\bar{S}_y = \sum_k S_y^{(k)}$. We recover the standard equations describing the radiation damping effect with a rate of $\frac{4g^2}{\kappa}\bar{S}_{x,y}$. Note here the unusual sign convention of this term since the thermal equilibrium point of the Bloch ball is the south pole and not the north pole of the Bloch sphere. This analysis also highlights a difference between the radiation damping and the Purcell effect since this latter occurs at rate $\frac{4g^2}{\kappa}$ [see Eq. (4) for $\Delta_j = 0$] even when $\bar{S}_{x,y} = 0$. Finally, note that the bad-cavity limit leads to a standard optimal control problem in magnetic resonance [1,80], which was solved, e.g., in [65].

III. OPTIMAL CONTROL OF A SPIN ENSEMBLE

A. The general procedure

We propose in this section a general procedure to design optimal-control fields in a dynamical system governed by Eq. (3). The inspection of the system (3) clearly shows that the control fields ω_X and ω_Y only change the time evolution of the quadratures X and Y and not directly the spin dynamics, which can only be modified in a two-step process. The two control fields can be expressed in terms of X and Y through the response function of the cavity:

$$\omega_X = \dot{X} + \frac{\kappa}{2}X + \sum_j 2g_j S_y^{(j)},$$

$$\omega_Y = \dot{Y} + \frac{\kappa}{2}Y - \sum_j 2g_j S_x^{(j)}. \tag{8}$$

For fast changing cavity fields, we observe in Eq. (8) that the time derivative of $X(t)$ and $Y(t)$ diverges and so do the control amplitudes ω_X and ω_Y.

The design process of the control fields can be decomposed into three different steps. We first determine the time evolution of $X(t)$ and $Y(t)$ to realize a given control task on the spin system. Note that this control issue is a standard control problem of a spin ensemble with offset (the parameters Δ_j) and field (the parameters g_j) inhomogeneities (see Refs. [1,12–14] for a series of results on the subject). We compute numerically, in a second stage, $\sum_j g_j S_x^{(j)}$ and $\sum_j g_j S_y^{(j)}$ with the last three equations of (3). This step can be neglected in the low-coupling limit ($g_j \simeq 0$). The fields ω_X and ω_Y are finally obtained with Eq. (8). The only mathematical constraint of this procedure relies on the fact that $X(t)$ and $Y(t)$ must be differentiable functions. This assumption will be satisfied by expanding X and Y on a specific function basis. Experimental limitations on the control fields will be discussed in Sec. IV.

Another option for the optimization process is to consider the dynamical system as a whole and to define a control objective in terms of the spin and the cavity coordinates. This approach was not used in this work for two main reasons. Due to the nonlinear character of the dynamics, it is no longer possible to define straightforwardly universal rotation pulses [13], i.e., rotations which do not depend on the initial state of the spin. Such rotations are an essential building block of spin echo or CPMG sequences [51,81]. In addition, we have observed that the corresponding control landscape admits many local extrema which prevent a fast convergence of the algorithm.

We show below on different benchmark examples how to control the spin ensemble. For the sake of generality, all the parameters are expressed in dimensionless units in Sec. III. A dimensional analysis can be used to determine the physical units of the different coefficients. If t_f denotes the real control time then $t \mapsto t \times t_f$, $\kappa \mapsto \kappa/t_f$, $\omega_{X,Y} \mapsto \omega_{X,Y}/t_f$, $g \mapsto g/t_f$, and $\Delta_j \mapsto \Delta_j/t_f$. Note that the X, Y and the $\vec{S}$ variables remain dimensionless.

B. Bump pulses

The first control sequence is aimed at reproducing the effect of a Dirac pulse on a spin system [51,52]. Dirac pulses are generally approximated by square pulses with an area
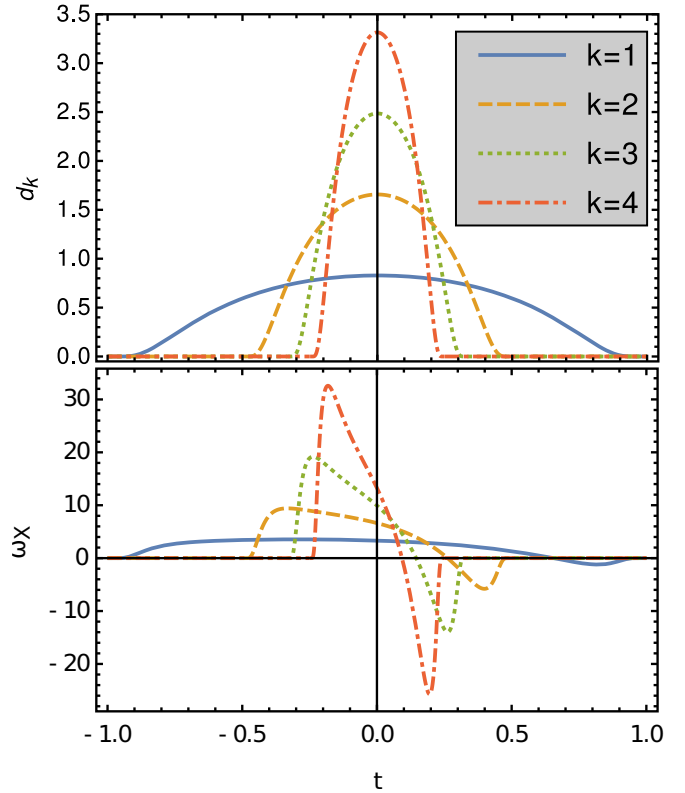

FIG. 2. Top: Sequence of functions $d_k(t)$ with a compact support converging to the Dirac distribution for $k = 1, 2, 3,$ and 4. Bottom: Plot of the corresponding control field ω_X with $\kappa = 4$ (the back-action from the spin system is neglected). Dimensionless units are used.

corresponding to the rotation angle induced by the field. Here, square pulses are not suited to the control process because their derivatives are singular distributions. Instead we propose to use the space of infinitely smooth bump functions of compact support [82], as displayed in Fig. 2. They have the property to be infinitely differentiable and to go to zero on the boundaries of their support. We introduce the set of functions $(d_k)_{k \in \mathbb{N}}$ defined by

$$d_k(t) = Ake^{1/(k^2t^2-1)}\mathbb{I}_{[-1/k,1/k]}(t), \tag{9}$$

where $\mathbb{I}_I$ is the indicator function on the interval I (this function takes the value 1 for elements of I and 0 outside). The bump functions satisfy

$$\lim_{k \to \infty} d_k = \delta.$$

The pulse duration t_f is set by the parameter k, $t_f = 2/k$. The normalization factor A is chosen so that $\int_{-1/k}^{1/k} d_k(t)dt = 1$. It can be expressed in terms of Whittaker's function: $A = \sqrt{\pi/e}W_{-1/2,1/2}(1) = 0.44399\cdots$.

An approximate Dirac pulse is applied to the spin system in the x direction if $X(t) = \theta d_k(t)$, where θ is the rotation angle induced by the pulse. A specific value of k is chosen. Using Eq. (6), this leads to the following control field ω_X:

$$\omega_X(t) = \theta Ak\left(\kappa - \frac{2k^2t}{(k^2t^2-1)^2}\right)e^{1/(k^2t^2-1)}$$

$$\times \mathbb{I}_{[-1/k,1/k]}(t) + \sum_j 2g_j S_y^{(j)}. \tag{10}$$

Figure 2 shows an example of different pulse sequences. This family of pulses is called hereafter *bump pulses*.

C. Design of optimal-control fields

More general control protocols can be designed along the same method. We consider the excitation and the inversion of the spin ensemble with different offset and field inhomogeneities. These robust pulse sequences are nowadays standard in magnetic resonance [1,12–14,80,81] either for point-to-point transformations or universal rotations. We investigate below this second class of pulses. The optimization procedure requires the introduction of a figure of merit $\mathcal{F}$ to maximize at time $t = t_f$. For the stability of numerical optimization, we come back to the Schrödinger picture and matrices of SU(2) are used to describe the rotation of each spin [13]. In this setting, $\mathcal{F}$ can be expressed as follows:

$$\mathcal{F} = \frac{1}{2N} \sum_{j=1}^{N} \text{Re}(\text{Tr}[U_f^\dagger U_j(t_f)]), \qquad (11)$$

where U_f is the target evolution operator for each spin and $U_j(t_f)$ the propagator at time $t = t_f$ of the spin j. The procedure is illustrated by two specific examples, namely $\pi/2$ and π rotations around the y axis, which correspond to the following unitary matrices:

$$U_\pi = \begin{pmatrix} 0 & -1 \\ 1 & 0 \end{pmatrix}, \quad U_{\pi/2} = \frac{1}{\sqrt{2}} \begin{pmatrix} 1 & -1 \\ 1 & 1 \end{pmatrix}. \qquad (12)$$

A peculiar analytical expression for the quadratures X and Y is chosen to design experimentally relevant control fields. They are parametrized as follows:

$$X = A(t) \cos[\varphi(t)],$$
$$Y = A(t) \sin[\varphi(t)], \qquad (13)$$

with

$$A(t) = A_0 \exp\left(\frac{1}{(2t-1)^p - 1}\right) \mathbb{I}_{[0,1]}(t),$$
$$(14)$$
$$\varphi(t) = \frac{a_0}{2} + \sum_{n=1}^{N_F} a_n \cos(2\pi n t) + b_n \sin(2\pi n t),$$

where A_0 is a normalization factor setting the pulse energy, p is an arbitrary odd number, and $\{a_n, b_n\}_{n=0...N_F+1}$ is the set of $2(N_F + 1)$ parameters to optimize. Numerical computations have been performed for two different situations. We first consider a uniform offset distribution in the interval $\Delta_j \in [-30, 30]$ and a constant coupling strength, $g = g_0 = 1$. In a second example, we assume that all the spins have the same frequency and that the parameter g is given by $g = g_0(1 + \alpha)$ with $\alpha \in [-0.3, 0.3]$. In the two cases, the control time is set to 1. Different pulse shapes are plotted in Fig. 3. The values of the pulse parameters are gathered in the Appendix. Note the more than 10 times larger amplitudes obtained for the pulses ω_X and ω_Y with respect to the ones of bump pulses in Fig. 2. A robust pulse against both offset and coupling-strength inhomogeneities can also be designed along the same lines but at the price of a longer control time or a larger pulse energy.
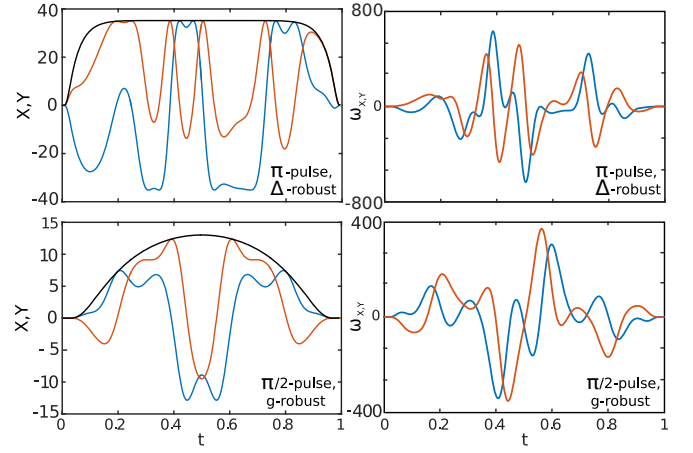

FIG. 3. Left: Optimized π (top) and $\pi/2$ pulses (bottom) robust against offset or coupling-strength distribution. X, Y, and $(X^2 + Y^2)^{1/2}$ are displayed respectively in red (dark gray), blue (black), and black solid lines. Right: Plot of the corresponding control fields ω_X and ω_Y. Dimensionless units are used. The parameter κ is set to 4.

IV. NUMERICAL RESULTS

A. Low-cooperativity regime

We investigate an example in the low-cooperativity regime reproducing recent experiments in ESR [47–50]. The measured signal in the cavity is an echo signal in X and Y produced by a standard Hahn sequence [51,53] of the form $(\pi/2)_y - \tau - (\pi)_y - \tau$, where τ is the echo time. This sequence is repeated several times at a rate $\gamma_r = 10$ Hz. In these experiments, the offset distribution ($\simeq$MHz) is wider than the cavity bandwidth ($\simeq$kHz). The spin polarization due to the repetition of the experiment reduces by several orders of magnitude the offset bandwidth contributing to the signal. Simulations are thus performed with an effective spin distribution which depends on the polarization $p = 1 - \exp[-1/(\gamma_r T_1^p)]$. The relaxation times are taken to be $T_1 = 3$ s, $T_2 = 1.7$ ms, and $T_1^p \simeq 100$ ms for $\Delta = 0$. Here, the Purcell rate provides the time required for a spin to relax toward its ground state. The spin does not reach the thermal equilibrium point between two repetitions. We assume that the initial distribution is approximately uniform on the interval ± 1.9 MHz with a total number of spins $N = 13\,500$. We also set $\kappa = 9.8 \times 10^5$ s^{-1} and $g_0/(2\pi) = 424$ Hz. With such parameters, the effective spin distribution is approximately Lorentzian of full width at half maximum (FWHM) $\Omega_p = 159.15$ kHz. The effective number of spins N_{eff}, i.e., the maximum number of spins which can be excited, is defined by

$$N_{\text{eff}} = N \int_{-\infty}^{+\infty} p(\Delta) d\Delta \simeq 940. \qquad (15)$$

N_{eff} can also be expressed in terms of the spin components as $N_{\text{eff}} = \bar{S}_z(t = 0^-)$ where $t = 0$ is the time at which the $\pi/2$ pulse of the echo sequence is applied. In this example, the cooperativity parameter $C = \frac{2N_{\text{eff}} g_0^2}{\kappa \Omega_p}$ is on the order of 0.01.

Following Refs. [47–50], we finally define the number of spins N_{spins} which are effectively excited by the control sequence applied in the interval $[0, t_f]$ and which therefore

contribute to the echo signal:

$$N_{\text{spins}} = \bar{S}_z(t = 0^-) - \bar{S}_z(t_f). \qquad (16)$$

For a perfectly selective $\pi/2$ pulse of bandwidth Ω_c, N_{spins} can also be estimated as

$$N_{\text{spins}} = N \int_{-\Omega_c/2}^{+\Omega_c/2} p(\Delta)d\Delta. \qquad (17)$$

In order to improve the sensitivity of the experiment, we are interested in maximizing the signal-to-noise ratio (SNR) associated with the echo signal in the cavity. The SNR for a single echo can be defined as follows [47]:

$$\text{SNR} = \sqrt{\frac{\int_{\text{echo}} X^2(t)dt}{\Delta X^2}}, \qquad (18)$$

where only the echo along the X direction is accounted for. At a temperature close to 0 K, the noise ΔX is estimated to be on the order of 1/2, which corresponds to the electromagnetic quantum fluctuations in the cavity; all the other noise sources are neglected [47–50]. The number of excited spins N_{min} for a SNR of 1 is given by $N_{\text{min}} = N_{\text{spins}}/\text{SNR}$ and will be used with the SNR to estimate the efficiency of the excitation process and the sensitivity of the detection.

We first investigate the robustness of the excitation process against offset and coupling-strength inhomogeneities for the bump, square, and g-robust pulses. The g-robust control sequence is determined by computing X and Y from Eqs. (13) and (14) with parameters in Table IV. The square pulses correspond to very short square pulses in ω_X and ω_Y. Note that the square pulses are highly deformed by the response function of the cavity. They were used experimentally, e.g., in [47], and they will be considered below as a reference of the control process. The spins are initially assumed to be along the z axis with a polarization given by the Purcell effect and interacting with a cavity with zero photons. We neglect in the different numerical simulations the relaxation times T_1 and T_2. As could be expected, we observe in Fig. 4 that the efficiency of bump fields is preserved for a wide range of offset frequencies, while a very good fidelity against variation of the g parameter is achieved on resonance for the g-robust pulse. Bump and g-robust solutions lead to a more robust control protocol than the standard square pulses.

As a second point of comparison, we study the performance of g-robust, bump, and square pulses in the maximization of the SNR. For each control sequence, we consider two cases, one corresponding to a constant $g = g_0$ distribution and the second to inhomogeneities of the form $g = g_0(1 + \alpha)$, with $\alpha \in [-0.3, 0.3]$. We also simulate ideal rotations on the spin system in order to estimate the maximum echo signal that can be reached with the spin distribution. The numerical results are displayed in Fig. 5, which shows the echo signal observed with the different pulses. For the sake of comparison, the duration of the bump pulses is the same as the one of g-robust fields (better results could be obtained with shorter bump pulses). An echo with a higher amplitude and a shorter time is achieved with the optimal solutions. We observe that the area of the different echoes in Fig. 5 is roughly the same for the different excitations. However, due to the shorter echo, the SNR is indeed increased with the optimal pulses.
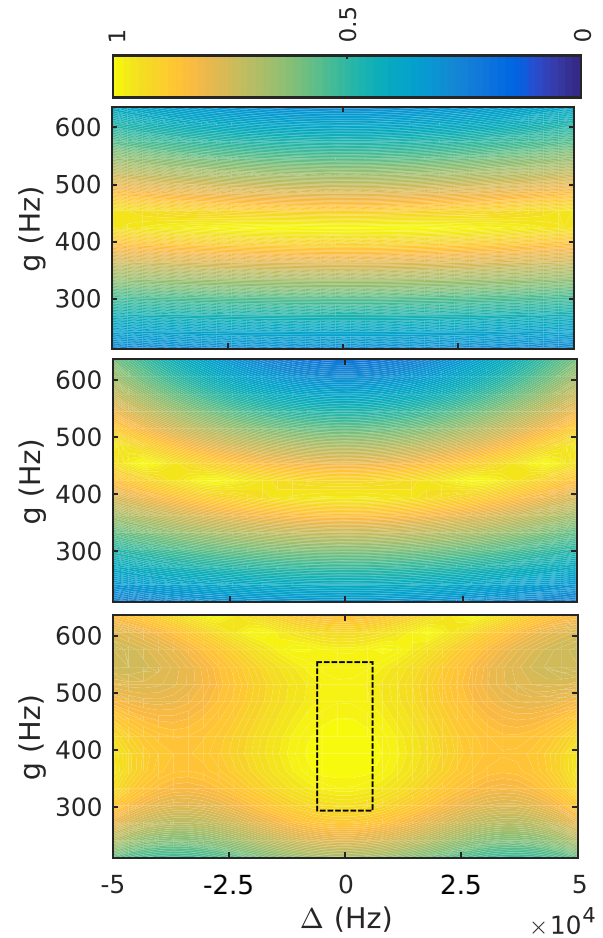

FIG. 4. Robustness of a $\pi/2$ excitation process against coupling strength g and offset Δ inhomogeneities of a bump pulse (top), a square pulse (middle), and a g-robust pulse (bottom). The rectangle in dashed lines indicates the spins used in the optimization. In order to provide a fair comparison, we fix the maximum value of X during the pulse. The pulse duration is set to satisfy this constraint: $t_{\text{square}} = 1\ \mu\text{s}$, $t_{\text{bump}} = 2t_k = 3.9\ \mu\text{s}$, and $t_{\text{g-robust}} = 19.5\ \mu\text{s}$.

The last point concerns the minimum number of spins N_{min} per echo with a SNR of 1 which can be excited by the different control protocols. As can be seen in Fig. 6, this minimum number is on the order of 260 spins with a square pulse of duration 1 μs [47,50]. In the case of Fig. 6, we show that a smaller number of spins for a SNR of 1 can be excited with bump pulses. N_{min} is on the order of 100 for a 15 μs long control process. This result is not obvious since bump pulses lead to a higher SNR but at the price of a larger number of excited spins. In other words, the control time $t_k = 1/k$ has to be adjusted to improve the selectivity of the excitation process without reducing drastically the SNR. In this case, g-robust $\pi/2$ pulses are not good candidates for the minimization of N_{min} due to their strong robustness.

As a second example, we consider a CPMG sequence in which a series of π pulses is applied periodically [51,81] with a period T after the excitation process. We assume a perfect initial $\pi/2$ excitation of the spin ensemble and the different relaxation effects are accounted for. The total SNR after M_r
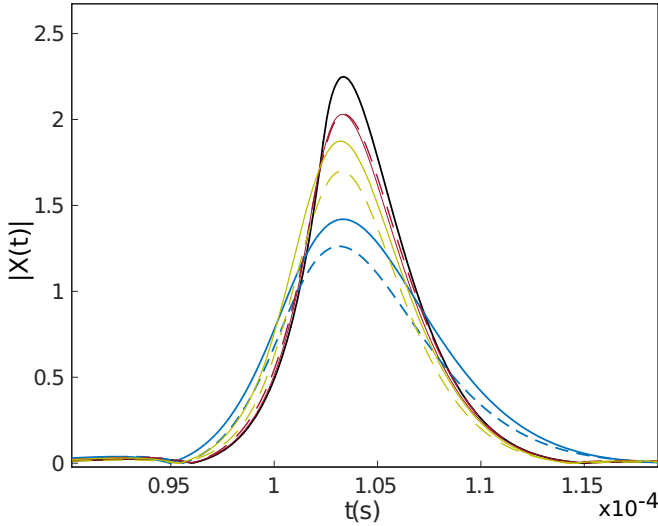
FIG. 5. Comparison of the echo signal in X for square pulses (in blue or dark gray), for bump pulses (in green or light gray), and for g-robust pulses (in red or gray). The physical limit with ideal spin rotations is displayed in black. The solid and dashed lines depict respectively the echo signal without and with g inhomogeneities. The pulse duration is set to $1\,\mu$s. X is expressed in dimensionless units.

echo signals can be expressed as

$$\mathrm{SNR}_{M_r} = \sqrt{\sum_k^{M_r} \mathrm{SNR}(k)^2}, \qquad (19)$$

where $\mathrm{SNR}(k)$ is the SNR of the kth echo. The parameters of the different CPMG sequences are given in Table I. The time T has been fixed to its minimum value for each pulse sequence. Table I gives the normalized SNR for one echo and for the whole CPMG sequence.

We observe in Table I that the g-robust pulses give a better SNR than the bump pulses. A noticeable enhancement of 25% is also obtained with respect to the square pulses. The results achieved with the two optimal solutions are in addition very close to the physical limit of an ideal spin echo sequence. The
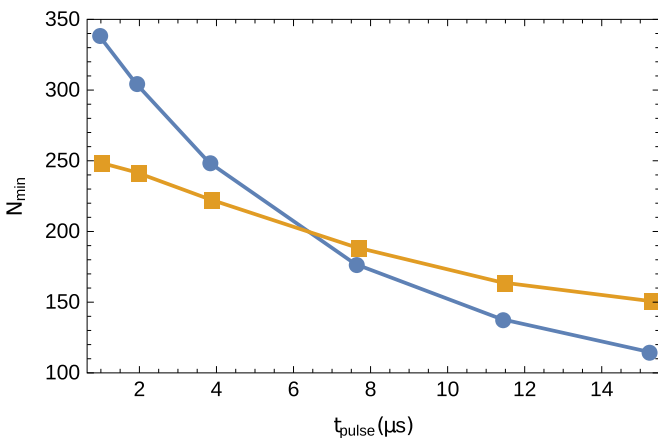

FIG. 6. Number of spins $N_{\min}$ per echo for bump (blue or dark gray) and square (orange or light gray) ω_X pulses of duration t_{pulse}. The parameter κ is set to $9.8 \times 10^5\,\mathrm{s}^{-1}$.

TABLE I. Parameters of the different CPMG sequences. The physical limit corresponds to ideal π rotations for all the spins of the ensemble. M_r indicates the maximum number of echoes which can be observed. The number of spins $N_{\min}$ for a SNR of 1 is computed for the first 100 echoes of the sequence.

π pulse	$\min(t_f)$ (s)	M_r	$\frac{\mathrm{SNR}_1}{\mathrm{SNR}_1^{\max}}$	$\frac{\mathrm{SNR}_{M_r}}{\mathrm{SNR}_{M_r}^{\max}}$	$N_{\min}$
Phys. limit	1.3×10^{-5}	321	1	1	55
Bump	3.69×10^{-5}	240	0.907	0.957	65
g robust	3.8×10^{-5}	231	0.967	0.918	67
Square	6.1×10^{-5}	160	0.754	0.406	94

improvement is even more striking for a CPMG sequence for which the gain is on the order of 60%. Due to its short duration which allows a larger number of repetitions, the bump pulse gives in this case the best result.

B. The high-cooperativity regime

We investigate in this section the controlled dynamics of a system in the high-cooperativity regime ($C \gg 1$) [83,84]. For that purpose, we consider a new set of parameters: $N = 135\,000$, $\gamma_r = 100$ Hz, and $g_0/(2\pi) = 4240$ Hz. This leads to $N_{\mathrm{eff}} = 2916$, $\Omega_p = 310$ kHz, and $C = 27$. The coupling strength g is taken as a constant, $g = g_0$, and we neglect the relaxation times T_1 and T_2. Figure 7 illustrates the dynamics induced by Δ-robust and square pulses. The duration of each pulse is set to $1\,\mu$s. Robust pulses are computed with the parameters presented in Tables II and III. Figure 7 clearly shows that the back-action of the spin dynamics onto the control field given by Eq. (8) cannot be neglected. The field is different from zero during the whole control time and in particular between the $\pi/2$ and π pulses.

An echo signal occurs in the cavity at $t = 10^{-4}$ s. The shape of the echo is preserved with the optimal pulse, while a deformed echo with many small bumps is observed in the standard case. Furthermore, the intensity of the echo and the SNR are respectively increased by a factor 10 and 100. For a SNR of 1, we obtain $N_{\min} = 43$ and $N_{\min} = 53$ for the optimal and square pulses. The same observation can be made on the spin dynamics in Fig. 7. In contrast to the variations produced

TABLE II. List of parameters for a Δ-robust $(\pi/2)_y$ universal rotation.

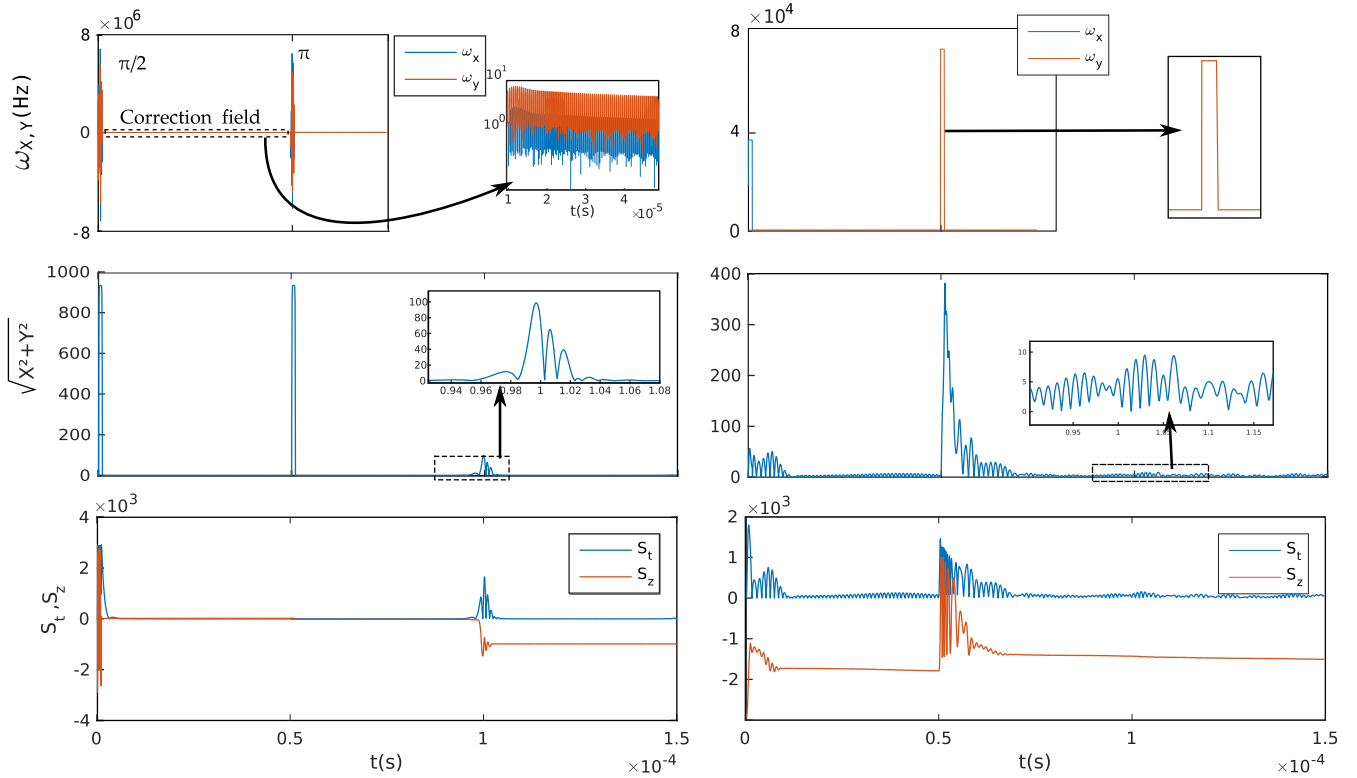| p		10	
t_f		1	
$\mathcal{F}$		0.9993	
n	a_n		b_n
0	2.48502852519278		0
1	-0.614602837937966		0.0222236529656774
2	-0.146403432037310		-0.326319502810118
3	0.249569148521250		0.212035090021068
4	-0.380514318815982		-0.294315446425150
5	-0.850981648334035		0.292006472615227
6	0.00534202375558939		-0.284521506361719
7	-0.445742825754110		-0.00924269034857846

FIG. 7. Spin echo sequence for Δ-robust (left) and square pulses (right). The top panels display the control fields. Note the correction field applied between the $\pi/2$ and π rotations in the first case. Time evolution of $\sqrt{X^2 + Y^2}$ (middle) and of the transverse $S_t = \sqrt{S_x^2 + S_y^2}$ and longitudinal S_z spin state. Unless specified, dimensionless units are used.

by the square pulses, a perfect excitation can be seen with the optimal control, $S_z \simeq 0$ for $0 < t < 10^{-4}$. A strong relaxation due to the radiation damping occurs during the two echoes. This signature of the high-cooperativity regime can be observed when $\bar{S}_x$ and $\bar{S}_y$ are very large.

V. CONCLUSION

In this work, we have applied quantum-control techniques to an inhomogeneous spin ensemble coupled to a cavity. We have described a general optimization procedure allowing us to implement standard Hahn and CPMG sequences in

the presence of offset and coupling-strength inhomogeneities. Relevant experimental values in ESR have been used for the numerical simulations. Different control strategies extending from bump pulses to g-robust fields have been derived. The relative advantages of the different solutions have been discussed in the low and high cooperativity regimes. Their superiority in terms of SNR and sensitivity over the standard square pulses has been demonstrated. In the experimental setup under study, the numerical results show that a good compromise is provided by the bump pulses which combine simplicity, efficiency, and robustness against offset inhomogeneities. Their short duration is also a key factor for the enhancement of the SNR by CPMG sequences.

TABLE III. List of parameters for a Δ-robust $(\pi)_y$ universal rotation.

p	10	
t_f	1	
$\mathcal{F}$	0.9997	
n	a_n	b_n
0	3.6552961005	0
1	-0.1862900729	0.3016414772
2	0.1569621446	0.9517460473
3	0.886144687	-0.5237345127
4	-0.3948819182	0.439535574
5	-0.362518991	-0.261853447
6	0.1747816746	0.2785205439
7	0.0332864557	0.0097613015

TABLE IV. List of parameters for g-robust $(\pi/2)_y$ (left) and $(\pi)_y$ (right) universal rotations. The b_n parameters are fixed to 0.

p	2	p	2
t_f	1	t_f	1
$\mathcal{F}$	0.999	$\mathcal{F}$	0.999
n	a_n	n	a_n
0	1.45730821080502	0	1.05923686097438
1	-1.90458549438015	1	-1.06434468127802
2	0.471852675517646	2	0.197782131275470
3	-0.164591020002767	3	-0.985850874873962
4	0.691022251640240	4	-0.680625181005274
		5	-0.680625181005274

These results confirm the key role that OCT could play in the near future for the detection of a single spin in ESR. Finally, we point out that more general pulse sequences could also be used to improve the efficiency of the overall process. An example is given by the cooperative pulses, a set of individual pulses which are designed to compensate each other's imperfections [85,86]. Recent works have shown their efficiency in a standard Hahn echo sequence. As a further step, it would be interesting to estimate the performance of such pulses in the maximization of the SNR or the minimization of spins per echo.

APPENDIX: PARAMETERS OF OPTIMAL PULSES

Tables II, III, and IV provide the different sets of parameters for the optimal pulses used in this work.

[1] S. J. Glaser, U. Boscain, T. Calarco, C. Koch, W. Kockenberger, R. Kosloff, I. Kuprov, B. Luy, S. Schirmer, T. Schulte-Herbrüggen, D. Sugny, and F. Wilhelm, Eur. Phys. J. D **69**, 279 (2015).

[2] C. Brif, R. Chakrabarti, and H. Rabitz, New J. Phys. **12**, 075008 (2010).

[3] D. Dong and I. A. Petersen, IET Control Theory A. **4**, 2651 (2010).

[4] C. Altafini and F. Ticozzi, IEEE Trans. Automat. Control **57**, 1898 (2012).

[5] D. D'Alessandro, *Introduction to Quantum Control and Dynamics* (Chapman and Hall, Boca Raton, 2008).

[6] S. A. Rice and M. Zhao, *Optimal Control of Molecular Dynamics* (John Wiley and Sons, New York, 2000).

[7] B. Bonnard and D. Sugny, *Optimal Control in Space and Quantum Dynamics*, AIMS Applied Mathematics, Vol. 5 (AIMS, Springfield, 2012).

[8] N. Khaneja, T. Reiss, C. Kehlet, T. Schulte-Herbrüggen, and S. J. Glaser, J. Magn. Reson. **172**, 296 (2005).

[9] D. M. Reich, M. Ndong, and C. P. Koch, J. Chem. Phys. **136**, 104103 (2012).

[10] J. Werschnik and E. K. U. Gross, J. Phys. B **40**, R175 (2007).

[11] P. Doria, T. Calarco, and S. Montangero, Phys Rev. Lett. **106**, 190501 (2011).

[12] K. Kobzar, T. E. Skinner, N. Khaneja, S. J. Glaser, and B. Luy, J. Magn. Reson. **170**, 236 (2004).

[13] K. Kozbar, S. Ehni, T. E. Skinner, S. J. Glaser, and B. Luy, J. Magn. Reson. **225**, 142 (2012).

[14] K. Kozbar, T. E. Skinner, N. Khaneja, S. J. Glaser, and B. Luy, J. Magn. Reson. **194**, 58 (2008).

[15] H. Rabitz and G. Turinici, Phys. Rev. A **75**, 043409 (2007).

[16] C. Chen, D. Dong, R. Long, I. R. Petersen, and H. A. Rabitz, Phys. Rev. A **89**, 023402 (2014).

[17] J. S. Li and N. Khaneja, IEEE Trans. Automat. Control **54**, 528 (2009).

[18] J. Ruths and J. S. Li, J. Chem. Phys. **134**, 044128 (2011).

[19] J. Ruths and J. S. Li, IEEE Trans. Automat. Control **57**, 2021 (2012).

[20] D. Daems, A. Ruschhaupt, D. Sugny, and S. Guérin, Phys. Rev. Lett. **111**, 050404 (2013).

[21] J. Somlói, V. A. Kazakov, and D. J. Tannor, Chem. Phys. **172**, 85 (1993).

[22] W. Zhu, J. Botina, and H. Rabitz, J. Chem. Phys. **108**, 1953 (1998).

[23] M. Lapert, Y. Zhang, M. Braun, S. J. Glaser, and D. Sugny, Phys. Rev. Lett. **104**, 083001 (2010).

[24] M. Lapert, Y. Zhang, M. Janich, S. J. Glaser, and D. Sugny, Sci. Rep. **2**, 589 (2012).

[25] E. Van Reeth, M. Lapert, H. Ratiney, S. J. Glaser, and D. Sugny, Pac. J. Math. Ind. **9**, 9 (2017).

[26] E. Van Reeth, H. Ratiney, M. Tesch, D. Grenier, O. Beuf, S. J. Glaser, and D. Sugny, J. Magn. Reson. **279**, 39 (2017).

[27] P. M. Lefebvre, E. Van Reeth, H. Ratiney, O. Beuf, E. Brusseau, S. Lambert, S. J. Glaser, D. Sugny, D. Grenier, and K. Tse Ve Koon, J. Magn. Reson. **281**, 82 (2017).

[28] S. Conolly, D. Nishimura, and A. Macovski, IEEE Trans. Med. Imag. **5**, 106 (1986).

[29] I. I. Maximov, M. S. Vinding, H. Desmond, N. C. Nielsen, and N. J. Shah, J. Magn. Reson. **254**, 110 (2015).

[30] I. I. Maximov, J. Salomon, G. Turinici, and N. C. Nielsen, J. Chem. Phys. **132**, 084107 (2010).

[31] M. H. Goerz, T. Calarco, and C. P. Koch, J. Phys. B **44**, 154011 (2011).

[32] A. Garon, S. J. Glaser, and D. Sugny, Phys. Rev. A **88**, 043422 (2013).

[33] N. Khaneja, R. Brockett, and S. J. Glaser, Phys. Rev. A **63**, 032308 (2001).

[34] D. Sugny and C. Kontz, Phys. Rev. A **77**, 063420 (2008).

[35] A. Schweiger and G. Jeschke, *Principles of Pulse Electron Paramagnetic Resonance* (Oxford University Press, Oxford, 2001).

[36] P. E. Spindler, Y. Zhang, B. Endeward, N. Gershernzon, T. E. Skinner, S. J. Glaser, and T. F. Prisner, J. Magn. Reson. **218**, 49 (2012).

[37] R. Prigl and U. Haeberlen, in *Advances in Magnetic and Optical Resonance*, Vol. 19, edited by W. S. Warren (Academic Press, Waltham, 1996), pp. 1–58.

[38] P. A. S. Cruickshank, D. R. Bolton, D. A. Robertson, R. I. Hunter, R. J. Wylde, and G. M. Smith, Rev. Sci. Instrum. **80**, 103102 (2009).

[39] G. Dridi, M. Lapert, J. Salomon, S. J. Glaser, and D. Sugny, Phys. Rev. A **92**, 043417 (2015).

[40] J. Wrachtrup and A. Finkler, J. Magn. Reson. **269**, 225 (2016).

[41] J. Wrachtrup, C. Von Borczyskowski, J. Bernard, M. Orritt, and R. Brown, Nature (London) **363**, 244 (1993).

[42] A. Gruber, A. Dräbenstedt, C. Tietz, L. Fleury, J. Wrachtrup, and C. v. Borczyskowski, Science **276**, 2012 (1997).

[43] S. Baumann, W. Paul, T. Choi, C. P. Lutz, A. Ardavan, and A. J. Heinrich, Science **350**, 417 (2015).

[44] D. Rugar, C. Yannoni, and J. Sidles, Nature (London) **360**, 563 (1992).

[45] D. Rugar, R. Budakian, H. Mamin, and B. Chui, Nature (London) **430**, 329 (2004).

[46] B. Julsgaard, C. Grezes, P. Bertet, and K. Molmer, Phys. Rev. Lett. **110**, 250503 (2013).

[47] A. Bienfait, J. J. Pla, Y. Kubo, M. Stern, X. Zhou, C. C. Lo, C. D. Weis, T. Schenkel, M. L. W. Thewalt, D. Vion, D. Esteve, B. Julsgaard, K. Molmer, J. J. L. Morton, and P. Bertet, Nat. Nanotechnol. **11**, 253 (2015).

[48] A. Bienfait, J. J. Pla, Y. Kubo, X. Zhou, M. Stern, C. C. Lo, C. D. Weis, T. Schenkel, D. Vion, D. Esteve, J. J. L. Morton, and P. Bertet, Nature (London) **531**, 74 (2016).

[49] A. Bienfait, P. Campagne-Ibarcq, A. H. Kiilerich, X. Zhou, S. Probst, J. J. Pla, T. Schenkel, D. Vion, D. Esteve, J. J. L. Morton, K. Moelmer, and P. Bertet, Phys. Rev. X **7**, 041011 (2017).

[50] S. Probst, A. Bienfait, P. Campagne-Ibarcq, J. J. Pla, B. Albanese, J. F. Barbosa, T. Schenkel, D. Vion, D. Esteve, K. Molmer, J. J. L. Morton, R. Heeres, and P. Bertet, Appl. Phys. Lett. **111**, 202604 (2017).

[51] M. H. Levitt, *Spin Dynamics: Basics of Nuclear Magnetic Resonance* (John Wiley & Sons, New York, 2008).

[52] R. R. Ernst, G. Bodenhausen, and A. Wokaun, *Principles of Nuclear Magnetic Resonance in One and Two Dimensions*, International Series of Monographs on Chemistry (Oxford University Press, Oxford, 1990).

[53] E. L. Hahn, Phys. Rev. **80**, 580 (1950).

[54] K. Rojan, D. M. Reich, I. Dotsenko, J.-M. Raimond, C. P. Koch, and G. Morigi, Phys. Rev. A **90**, 023824 (2014).

[55] J. L. Allen, R. Kosut, J. Joo, P. Leek, and E. Ginossar, Phys. Rev. A **95**, 042325 (2017).

[56] D. O. Krimer, B. Hartl, F. Mintert, and S. Rotter, Phys. Rev. A **96**, 043837 (2017).

[57] S. Deffner, J. Phys. B **47**, 145502 (2014).

[58] R. Fisher, F. Helmer, S. J. Glaser, F. Marquardt, and T. Schulte-Herbrüggen, Phys. Rev. B **81**, 085328 (2010).

[59] Q. Sun, R.-B. Wu, T.-S. Ho, and H. Rabitz, arXiv:1612.03988.

[60] A. de Freitas, L. Sanz, and J. M. Villas-Boas, Phys. Rev. B **95**, 115110 (2017).

[61] H. Haroche and J.-M. Raimond, *Exploring the Quantum: Atoms, Cavities, and Photons* (Oxford University Press, Oxford, 2006).

[62] E. T. Jaynes and F. W. Cummings, IEEE **51**, 89 (1963).

[63] R. Kubo, J. Phys. Soc. Jpn. **17**, 1100 (1962).

[64] N. Bloembergen and R. V. Pound, Phys. Rev. **95**, 8 (1954).

[65] Y. Zhang, M. Lapert, D. Sugny, and S. J. Glaser, J. Chem. Phys. **134**, 054103 (2011).

[66] W. S. Warren, S. L. Hammes, and J. L. Bates, J. Chem. Phys. **91**, 5895 (1989).

[67] M. P. Augustine, Prog. Nucl. Magn. Reson. Spec. **40**, 111 (2002).

[68] R. Azouit, A. Sarlette, and P. Rouchon, in *Proceedings of the 54th IEEE Conference on Decision and Control (CDC 2015), Osaka, 2015* (IEEE, Piscataway, NJ, 2015), pp. 6447–6453.

[69] R. Azouit, F. Chittaro, A. Sarlette, and P. Rouchon, Quantum Sci. Technol. **2**, 044011 (2017).

[70] B. Julsgaard and K. Mølmer, Phys. Rev. A **85**, 032327 (2012).

[71] J. Wang, H. M. Wiseman, and G. J. Milburn, Phys. Rev. A **71**, 042309 (2005).

[72] D. J. Atkins, H. M. Wiseman, and P. Warszawski, Phys. Rev. A **67**, 023802 (2003).

[73] E. Brion, L. H. Pedersen, and K. Molmer, J. Phys. A **40**, 1033 (2007).

[74] E. A. Sete, J. M. Gambetta, and A. N. Korotkov, Phys. Rev. B **89**, 104516 (2014).

[75] M. Tavis and F. W. Cummings, Phys. Rev. **170**, 379 (1968).

[76] M. C. Butler and D. P. Weitekamp, Phys. Rev. A **84**, 063407 (2011).

[77] V. V. Temnov and U. Woggon, Phys. Rev. Lett. **95**, 243602 (2005).

[78] C. J. Wood and D. G. Cory, Phys. Rev. A **93**, 023414 (2016).

[79] J. F. Collombeau, *Elementary Introduction to New Generalized Functions* (North Holland, Amsterdam, 1985).

[80] N. C. Nielsen, C. Kehlet, S. J. Glaser, and N. Khaneja, *Optimal Control Methods in NMR Spectroscopy*, Encyclopedia of Nuclear Magnetic Resonance (Wiley, New York, 2010).

[81] T. W. Borneman, M. D. Hürlimann, and D. G. Cory, J. Magn. Reson. **207**, 220 (2010).

[82] L. Schwartz, *Mathematics for the Physical Sciences* (Dover Books on Mathematics, Paris, 2008).

[83] B. C. Rose, A. M. Tyryshkin, H. Riemann, N. V. Abrosimov, P. Becker, H.-J. Pohl, M. L. W. Thewalt, K. M. Itoh, and S. A. Lyon, Phys. Rev. X **7**, 031002 (2017).

[84] A. Auffèves, D. Gerace, S. Portolan, A. Drezet, and M. F. Santos, New J. Phys. **13**, 093020 (2011).

[85] M. Braun and S. J. Glaser, J. Magn. Reson. **207**, 114 (2010).

[86] W. Kallies and S. J. Glaser, J. Magn. Reson. **286**, 115 (2018).